Special Feature: Advanced Thermal Management Technology for Developing the High-efficiency Vehicle

Research Report

Smart Design of Thermoelectric Materials for a Waste Heat Regeneration System

Hirofumi Hazama, Masato Matsubara, Yumi Masuoka and Ryoji Asahi

Report received on Jul. 3, 2018

ABSTRACT Thermoelectric generators (TEGs) can directly convert waste heat into useful electricity. Various applications, such as utilizing waste heat generated by vehicles, radiant heat produced in the steel making process, and solar energy, have been examined in recent years. The thermoelectric conversion efficiency of TEGs is characterized by the dimensionless figure of merit (*ZT*) for the thermoelectric materials they are constructed from. However, because of the intrinsic trade-off between high electrical conductivity and low thermal conductivity, it is not easy to dramatically increase *ZT*. The strategy used in the present study is based on conceptual ideas such as co-doping with donors and acceptors, crystallographic defects, and energy filtering, which may overcome this trade-off. These concepts are implemented by atomistic modifications in conventional thermoelectric materials, designed by first-principles calculations. In the present paper, we demonstrate three thermoelectric materials systems that have been designed and synthesized using this strategy. The results show a significant improvement in thermoelectric properties, legitimating and emphasizing the importance of design concepts based on physical and chemical insights.

KEYWORDS Material Design, Thermoelectric Material, Co-doping with Donors and Acceptors, Crystallographic Defects, Energy Filtering with Nanocomposite Phases

1. Introduction

Waste heat is the unused heat inevitably generated by automobile engines or power plants. Dissipated into the atmosphere, it limits the efficiency of thermodynamic processes and contributes to global warming. A thermoelectric generator (TEG) is a promising solution to these problems since it reuses waste heat, directly converting it into useful electricity. In particular, TEGs can be installed in limited spaces, and their power density is relatively high (on the order of 1 W/cm^2). Therefore, various applications of TEGs have been examined in recent years. One example is the automotive TEG. Crane et al. reported that a TEG mounted downstream of the catalytic converter on a vehicle produced 600 W of electrical power when the TEG hot side was heated by exhaust gas and its cold side was exposed to a coolant.[1] As a result, the relative improvement in fuel efficiency exceeded 1.2% at a vehicle speed of 110 kph. Another example is a waste heat recovery system in a steel making process demonstrated by Kuroki et al.[2] A TEG with dimensions of 2 m × 4 m produced approximately 9 kW from the radiant heat produced by casting slabs when the slab temperature and the distance between the slab and the TEG were 915°C and 2 m, respectively. Recently, we demonstrated a solar TEG with a water heating system with a high energy conversion efficiency.[3]

The thermoelectric efficiency of TEGs is characterized by the dimensionless figure of merit (*ZT*) for the thermoelectric (TE) material, which is defined as

$$ZT = \left(\sigma S^2 / \kappa\right) T , \tag{1}$$

where σ, S, κ, and T are the electrical conductivity, the Seebeck coefficient, the thermal conductivity, and the temperature, respectively. The average ZT (ZT_{ave}) obtained from the temperature of the cold side (T_c) and the hot side (T_h) of the TEG is required in order to estimate the TE efficiency. Here, ZT_{ave} is defined as

$$ZT_{ave} = \left(\int_{T_c}^{T_h} ZT dT \right) / \left(T_h - T_c\right) . \tag{2}$$

The ideal TE efficiency (η_{TEG}) is given by

$$\eta_{TEG} = \frac{T_h - T_c}{T_h} \times \frac{\left(1 + ZT_{ave}\right)^{1/2} - 1}{\left(1 + ZT_{ave}\right)^{1/2} + T_c / T_h} \quad . \qquad (3)$$

Note that ZT_{ave} and ΔT (= $T_h - T_c$) should be maximized to obtain a high η_{TEG}, but T_h and T_c are restricted by the TEG application. For example, for an internal combustion engine, T_h = 600°C for the exhaust gas and T_c = 30°C based on the coolant.[4,5] Therefore, increasing the ZT value for TE materials is a crucial topic when developing TEGs. **Figure 1** shows the T_h dependence of η_{TEG} (T_c = 30°C). At this juncture, the practical value of ZT_{ave} is approximately 1 at best for T_h = 600°C and T_c = 30°C, and thus η_{TEG} is approximately 10%.

When T_h is below 300°C, Bi_2Te_3-based materials are commonly used for TEGs because no materials with higher a ZT value have yet been found. Recently, the maximum ZT value for such materials has been increasing, e.g., 1.1 at 100°C (n-type)[6] and 1.86 at 47°C (p-type).[7] When T_h is approximately 600°C, $CoSb_3$-based materials have been found to exhibit ZT values of up to 1.7 at 577°C (n-type)[8] and 1.06 at 427°C (p-type).[9] Generally, a TEG consists of n- and p-type TE materials, which are electrically connected in series, as shown in **Fig. 2**. A high-efficiency TEG is therefore realized when both the n-type and p-type TE materials have a high ZT value. The efficiencies of TEGs using Bi_2Te_3- and $CoSb_3$-based materials were reported to be 7.2% at T_h = 280°C[2] and 8.4% at T_h = 600°C,[9] respectively. A segmented TEG consisting of Bi_2Te_3- and $CoSb_3$-based materials exhibited a higher efficiency of up to 12% at T_h = 576°C.[10] New TE materials are also under development, and have been found to exhibit a maximum ZT of 2.3 at 650°C (p-type PbTe-based material),[11] 2.1 at 727°C (p-type Cu_2S-based material),[12] and 2.0 at 500°C (p-type SnSe-based material).[13] However, toxicity, low oxidation resistance, and poor stability, which are inherent in TE materials, often hinder the practical application of such TEGs.

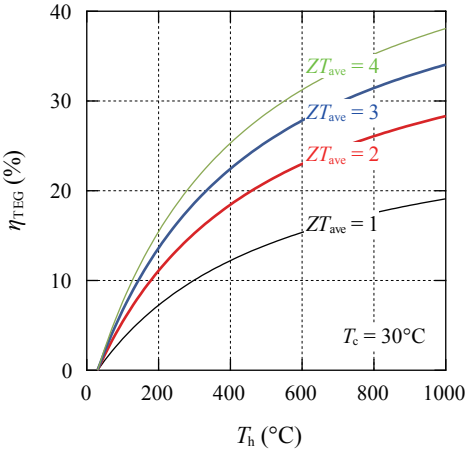

Fig. 1 Hot-side temperature (T_h) dependence of the ideal thermoelectric efficiency (η_{TEG}) of the TEG when the cold-side temperature (T_c) is 30°C. The ZT_{ave} is the average ZT from T_c to T_h for the thermoelectric materials.

Because of the intrinsic trade-off between the need for a high electrical conductivity and a low thermal conductivity, it is not easy to increase ZT dramatically. In the present paper, we introduce three conceptual ideas, i.e., co-doping with donors and acceptors,[14] crystallographic defects,[15] and energy filtering with nanocomposite phases,[16] as shown in Fig. 2. Crystallographic defects and nanocomposites act as phonon scattering centers and reduce κ drastically in some cases. Co-doping with donors and acceptors leads to the formation of local dipoles which can also give rise to a significant reduction in κ without reducing the carrier mobility. We have previously calculated the local dipole effect of co-doping for PbTe-based materials.[17] It was found that co-doping with donors and acceptors changed the band structure around the Fermi energy without changing the carrier concentration. Thus, it is possible to increase the power factor ($PF = \sigma S^2$). The nanocomposites of energy filter phases are also possible to increase PF due to the restriction of low energy carrier by those potential heights. These concepts are implemented by atomistic modifications in conventional TE materials, namely TiNiSn and Bi_2Te_3 compounds, which are designed by first-principles calculations. In the present paper, we demonstrate three TE materials that are designed and synthesized using this strategy in order to determine whether an improvement in TE properties can be realized.

2. Calculations and Experiments

We used the plane-wave projector augmented-wave (PAW) method[18,19] implemented in the Vienna ab initio

simulation package (VASP) code[20,21] for first-principles calculations. The generalized gradient approximation (GGA) was used for the exchange and correlation potential. A stable state for each model was determined by minimizing the total energy while relaxing the atomic positions and lattice constants using a reciprocal-space k-mesh with a spacing of less than 0.2 $Å^{-1}$ in each direction, and an energy convergence below 1×10^{-7} eV. The formation energy (*FE*) for substituting an element C for an element B in a compound AB is defined as $FE\,(\mathrm{AB} \rightarrow \mathrm{AC}) = [E\,(\mathrm{AC}) + \mu\,(\mathrm{B})] - [E\,(\mathrm{AB}) + \mu\,(\mathrm{C})]$, where E and μ are the total energy of the compound and the chemical potential of the element in metallic state, respectively. A more negative *FE* means that AC is more stable than AB.

The band structure for each model was calculated by the full-potential linearized augmented plane-wave (FLAPW) method. The electrical conductivity (σ) and the Seebeck coefficient (S) were calculated using the band structure with the Bloch-Boltzmann equations as

$$\sigma_E(\varepsilon, T) = e^2 N(\varepsilon)\, v^2(\varepsilon)\, \tau(\varepsilon, T), \tag{4}$$

$$\sigma(T) = \int \sigma_E(\varepsilon, T) \left[-\frac{\partial f(\varepsilon)}{\partial \varepsilon} \right] d\varepsilon, \tag{5}$$

$$S(T) = \frac{1}{eT\sigma(T)} \int (\in - \mu)\, \sigma_E(\varepsilon, T) \left[-\frac{\partial f(\varepsilon)}{\partial \varepsilon} \right] d\varepsilon, \tag{6}$$

where e, N, v, τ, f, and μ are the elementary charge, the density of states, the group velocity, the relaxation time, the Fermi function, and the chemical potential, respectively.

We synthesized TiNiSn- and Bi_2Te_3-based TE materials. The TiNiSn-based materials described in Secs. 3. 1 and 3. 2 were prepared in a radiofrequency (RF) furnace under an Ar atmosphere by first melting a mixture of Ti (Kojundo Chemical Laboratory Co., Ltd., purity 99.9%), Ni (99.9%), Sn (99.99%), Hf (98%), Zr (98%), Y (99.9%), Sb (99.99%), Co (99.99%), and Sc (Shin-Etsu Chemical Co., Ltd., 99.9%) grains in appropriate molar ratios. The obtained ingots were melted again in an RF furnace and were rapidly liquid-quenched on a single-roll Cu wheel, which reduced the impurity phases and compositional inhomogeneity. The quenched samples were ground to a powder and sintered at 1100°C for 15 min under a pressure of 50 MPa in a vacuum by employing the spark plasma sintering (SPS) technique. On the other hand, Bi_2Te_3-based materials, as described in Sec. 3. 3, were prepared as rectangular pellets pressed in a die after first mixing Bi (Kojundo Chemical Laboratory Co., Ltd., purity 99.999%) powder, Te (99.999%) powder, and Ga (99.99%) grains in appropriate molar ratios. The pellets were sealed in a vacuum quartz ampoule in order to prevent volatilization of the raw materials, and then melted for 4 h in a muffle furnace at 700°C. The obtained ingots were melted again and were rapidly liquid-quenched. The quenched samples were ground into powder and sintered at 450°C for 5 min under a pressure of 50 MPa in a vacuum by SPS. The sintered samples were sealed again in a vacuumed quartz ampoule and then heated at 400°C for 24 h in a muffle furnace. Based on the eutectic phase behavior of Ga_2Te_3–Bi_2Te_3, we employed quenching and post-annealing processing to control the size and homogeneity of the nanosized precipitations of the Ga_2Te_3 filter phases.

In order to measure the transport properties, synthesized samples were cut into bars with dimensions of 2-3 mm × 2-3 mm × 10 mm using a diamond wheel saw. The electrical conductivity, Seebeck coefficient and thermal conductivity below room temperature

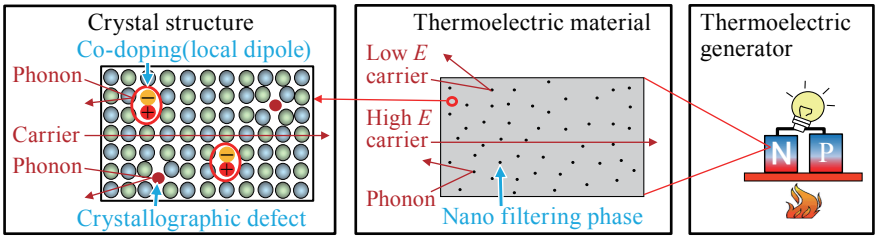

Fig. 2 Schematic diagram of a common TEG consisting of n- and p-type thermoelectric materials and the items to be studied for increasing *ZT* in the present paper.

were measured using a physical property measurement system (PPMS, Quantum Design, Inc.).

3. Results and Discussion

3. 1 Improvement of Power Factor Due to Co-doping with Donors and Acceptors

TiNiSn-based TE materials are attracting a great deal of interest because they contain no toxic elements and have a high ZT[14] value of around 600°C, which is similar to the temperature of automotive exhaust gas. Therefore, automotive TEGs using these materials have been investigated.[4,5] In this section, we introduce the co-doping effect of TiNiSn-based materials[14] as a case study.

Based on the concept that local dipoles formed by co-doping with donors and acceptors can reduce κ drastically while maintaining a high carrier mobility, we first narrowed down the co-doping candidates by performing calculations. We evaluated the *FE* value in order to clarify how easily co-doping can be achieved in TiNiSn. **Figure 3** shows the calculated *FE* value for different doped system in the $Ti_4Ni_4Sn_4$ supercell. The dopants were selected so that the charge neutrality of the material was maintained. Since YSb (simultaneous substitution of Y at Ti sites as an acceptor and Sb at Sn sites as a donor), ScSb, and CoSb co-dopants in TiNiSn have negative *FE* values, they may be stable, and their solubility limit may be high. In addition, we confirmed for ScSb (YSb) co-doping that the nearest neighbor configuration of Sc (Y) and Sb in the crystal shows the lowest *FE* by the calculations in the case of ScSb (YSb) doping. This means that forming local dipoles of Sc (Y) and Sb is more stable than separated monopoles of Sc (Y) or Sb.

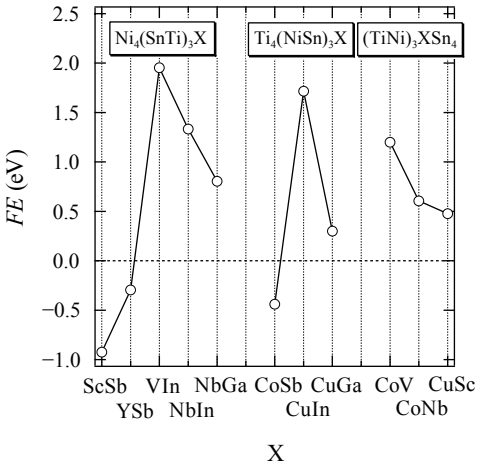

Fig. 3 Calculated formation energy (*FE*) for different co-doped states in the $Ti_4Ni_4Sn_4$ supercell.

In order to determine how the local dipoles produced by co-doping affects the TE properties due to a change in the band structure, we calculated *PF* using the $Ti_{32}Ni_{32}Sn_{32}$ supercell for the co-doping models. **Table 1** shows the calculated PF/PF_0 at 600 K for different 1% co-doped states in TiNiSn in the case of forming local dipoles.[14] The *PF* was evaluated from the calculated σ and S under the assumption that the relaxation time (τ) for each model is the same as that for TiNiSn. The *PF* for non-doped TiNiSn (PF_0) was used as the standard value for comparison. The YSb or ScSb co-doping is predicted to increase *PF* in comparison with non-doped TiNiSn.

We applied these co-dopants to a TiNiSn-based material, $Ti_{0.5}Zr_{0.25}Hf_{0.25}NiSn$, the *ZT* value for which is higher than that for TiNiSn due to the κ reduction by partial isovalent substitutions of Zr and Hf for Ti. The experimental results at 600 K, which were measured by RZ2001i of Ozawa Science Co. Ltd., are listed in Table 1. It was found that YSb or ScSb co-doping increased *PF* and CoSb co-doping lowered *PF*, which is consistent with the calculated results. **Figure 4** shows the temperature dependence of *ZT* for the non-doped, the 0.3% Sb-doped, and the 1% YSb co-doped $Ti_{0.5}Zr_{0.25}Hf_{0.25}NiSn$.[14] The doping concentrations for Sb and YSb in Fig. 4 were optimized so as to maximize *ZT*. Sb doping at Sn sites increased the *ZT* value due to the improvement of *PF* by optimization of the carrier concentration (n). When n is increased by introducing donors or acceptors into a TE material, e.g., substitution of Sb at Sn sites in TiNiSn, the electrical conductivity is increased, whereas

Table 1 Calculated and experimental PF/PF_0 at 600 K for different 1% co-doped states in TiNiSn.[14]

	Calculation (PF/PF_0)	Experiment (PF/PF_0)
Non-doped	1	1
1%CoSb	0.76	0.76
1%ScSb	1.12	1.44
1%YSb	1.15	1.74

the absolute value of the Seebeck coefficient (|*S*|) is generally inversely proportion to the natural logarithm of the electrical conductivity (ln *n*) as observed in the Jonker plot. Therefore, the *PF* improvement due to single-element doping is limited by the relation between |*S*| and ln *n*. Co-doping of YSb, however, realized a further improvement of *PF*, and thus, surprisingly, *ZT* was even better than the theoretical prediction. This discrepancy may result from a change in the relaxation time induced by co-doping, which was not considered by the present calculations. These observations lead to the conclusion that appropriate co-doping is an effective method for increasing *ZT*, apart from optimizing the carrier concentration.

3. 2 Reduction of Thermal Conductivity Due to Crystallographic Defects

One of the problems of TiNiSn-based materials is the inclusion of the expensive elements Hf and Zr, which are known to decrease the thermal conductivity. In this section, we introduce an alternative low-cost method to lower the thermal conductivity, i.e., crystallographic defects in the TiNiSn crystal.[15] Defects can lower κ drastically because they become phonon scattering centers. Several types of defects can be introduced into the crystal, e.g., vacancies, interstitials, and antisites, depending on the composition and synthesis process. We evaluated the *FE* value for several types of defects in TiNiSn crystals by modeling using the $Ti_{32}Ni_{32}Sn_{32}$ supercell. **Table 2** shows the calculated *FE* in the case of excess Ni in TiNiSn. V@Sn and V@Ti represent Sn and Ti vacancies, respectively. In addition, Ni@Ti and Ni@Sn represent substitutions of Ni for Ti and Ni for Sn, respectively. Interstitial Ni is an excess Ni atom at one of the vacancies in the TiNiSn crystal structure, as shown in **Fig. 5**. The *FE* value for the interstitial Ni defect is quite low, even though it is positive. The calculation results indicate that excess Ni atoms are preferentially located at interstitial vacancy sites, forming a weak bond with the TiNiSn crystal. This situation is similar to that for filled skutterudite materials, where the crystal structure has vacancy sites that are large enough to introduce different atoms that are weakly bonded to the original crystal framework. These foreign atoms scatter phonons and thereby reduce the thermal conductivity significantly while maintaining a high electron mobility by the rattling effect.[22] We thus expect a similar effect in TiNiSn with excess Ni.

We synthesized TiNiSn containing excess Ni in order to introduce interstitial Ni defects, and evaluated

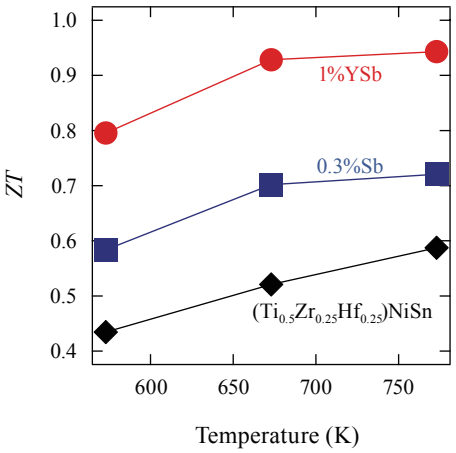

Fig. 4 Temperature dependence of *ZT* for the non-doped, the 0.3% Sb-doped, and the 1% YSb co-doped $Ti_{0.5}Zr_{0.25}Hf_{0.25}NiSn$.[14]

Table 2 Calculated formation energy (*FE*) and expansion ratio for the lattice constant (*a*) for different defect models in comparison with TiNiSn.

Model	*FE* (eV)	$\Delta a/a$ (%)
V@Sn	4.71	−0.09
V@Ti	3.97	−0.11
Ni@Ti	3.35	−0.16
Ni@Sn	3.02	−0.14
Interstitial Ni	0.19	0.11

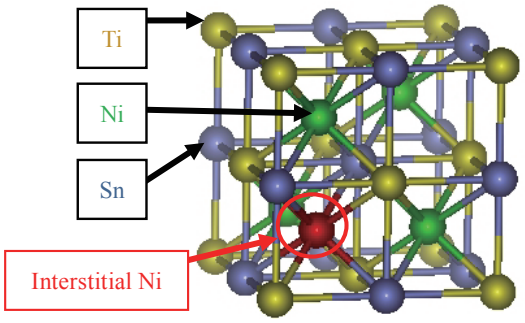

Fig. 5 Model of an interstitial Ni atom at one vacancy in the TiNiSn crystal structure.

the resulting TE properties. If the excess Ni occupies vacancy sites in TiNiSn, as shown in Fig. 5, the lattice constant (a) should increase, as predicted in Table 2. **Figure 6** shows the dependence of a and κ at 300 K on the Ni content (x), where $0.480 \leq x \leq 0.568$.[15] Here, a was determined by powder X-ray diffraction (XRD) patterns measured by a Rigaku RAD-2X using CuKα radiation, and x is the ratio of the amount of Ni to the total amount of Ti and Sn in the samples and was determined by inductively coupled plasma (ICP) spectrometry. Since a becomes larger as x increases, following Vegard's law, we found that excess Ni occupies vacancy sites in the TiNiSn crystal in the range of $0.480 \leq x \leq 0.540$. These interstitial Ni defects reduce κ, as shown in Fig. 6. In the case of the $x = 0.568$ sample, a is approximately the same as that for $x = 0.540$. This suggests that the solubility limit for Ni is around $x = 0.540$. Above this solubility limit, at $x = 0.568$, XRD patterns indicated the presence of $TiNi_2Sn$ precipitates, and the κ value was higher. **Figure 7** shows the temperature dependence of ZT for TiNiSn compounds.[15] The ZT value at $x = 0.540$ is the highest among the synthesized samples because of the reduced κ value and the increased PF value due to the presence of interstitial Ni defects. We thus confirmed the effectiveness of introducing crystallographic defects to improve ZT. Note that following our research, the effect of interstitial Ni defects in TiNiSn has been investigated in detail.[23] The significant reduction in κ for TiNiSn without the need for expensive elements such as Zr and Hr is an attractive approach for practical applications.

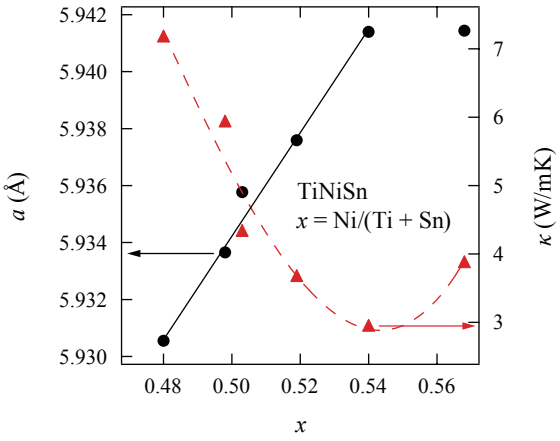

Fig. 6 Ni content (x) dependence of the lattice constant (a) and the thermal conductivity (κ) at 300 K for TiNiSn compounds ($0.480 \leq x \leq 0.568$).[15]

3. 3 Improvement of Power Factor by Energy Filtering Effect of Nanocomposites

Nanocomposites are also known to improve the ZT value for TE materials. In most cases, this increase is caused by phonon scattering, which reduces the κ value more than the PF value. Recently, modulation doping, i.e., the formation of nonuniform nanocomposites, is a popular method by which to increase the PF value due to increasing the carrier mobility.[24] In this section, we introduce nanocomposites of energy filtering phases in n-type Bi_2Te_3-based materials.[16] **Figure 8** shows a schematic diagram of the band offset between the filter phase and the TE material. In the

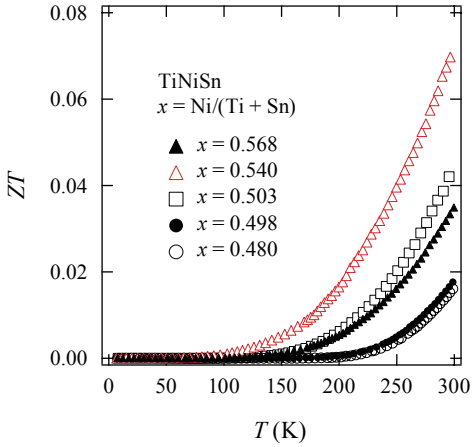

Fig. 7 Temperature dependence of ZT for TiNiSn compounds ($0.48 \leq x \leq 0.568$).[15]

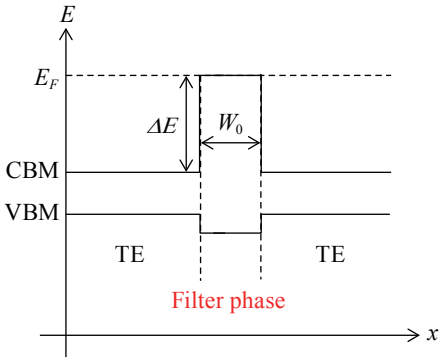

Fig. 8 Schematic diagram of the band offset between the filter phase and the thermoelectric (TE) material.

figure, CBM and VBM indicate the conduction band minimum and valence band maximum, respectively, and E_F, ΔE, and W_0 refer to the Fermi level of the TE material, the potential barrier height, and the size of the filter phase, respectively. The filtering effect originates from an asymmetry in the density of states around E_F for the TE material. To this end, we need to select filter phases with an appropriate value of ΔE, i.e., such that the CBM for the filter phase is aligned with the E_F for the TE material. Therefore, we must simultaneously control E_F for the TE material, and ΔE and W_0 for the filter phase in order to maximize the filtering effect. However, this is difficult to achieve with bulk materials.

In the case of n-type Bi_2Te_3, E_F can be shifted by approximately 0.2 eV above the CBM.[25] We therefore searched for a material with a low ΔE of approximately 0.2 eV and found that Ga_2Te_3 may be suitable as the filter phase. The ΔE value for Ga_2Te_3 with respect to the CBM of Bi_2Te_3 was estimated based on E_{core} obtained based on the Bi_2Te_3 and Ga_2Te_3 crystal structure models, E_b at the Bi_2Te_3/Ga_2Te_3 interface, and the experimentally determined bandgap (E_g) for Bi_2Te_3 and Ga_2Te_3. Here, E_{core} and E_b are the energy difference between the VBM and the Te 1s core level (Te_{1s}), and between the Te_{1s} levels for Ga_2Te_3 and Bi_2Te_3, respectively. **Figure 9** shows the band offset between Ga_2Te_3 and Bi_2Te_3 obtained by the calculations.[16] The value of ΔE was estimated to be 1.0 eV, which is larger than the expected value of 0.2 eV. However, we chose Ga_2Te_3 as the filter phase considering the tunneling effect and the possible reduction of the band gap of Ga_2Te_3 depending on the defect structure. Concerning the size of the filter phase, as W_0 increases, σ will decrease due to the decreasing transmittance of low energy electrons in the filter phase, whereas a smaller W_0 will reduce the energy filtering effect because electrons are only somewhat restricted because of tunneling in the filter phase.

We synthesized Bi_2Te_3 with nanosized Ga_2Te_3 regions and evaluated its TE properties. **Figure 10** shows a backscattered electron (BSE) image of the synthesized $Bi_{0.85}Ga_{0.15}Te_3$.[16] The sample was confirmed to contain homogeneously dispersed nanosized Ga_2Te_3 precipitates in Bi_2Te_3, and the average Ga_2Te_3 grain size was approximately 100 nm. **Figure 11** shows $|S|$ versus ln σ for $Bi_{2-x}Ga_xTe_3$ ($0 \le x \le 0.25$) at 300 K.[16] Since the relationship is linear, i.e., a Jonker plot, the maximum PF (PF_{max}) for Bi_2Te_3 is evaluated to be 1.75×10^{-3} W/mK^2. However, the presence of the nanosized Ga_2Te_3 precipitates in Bi_2Te_3 ($0.07 \le x \le 0.15$) increases the PF_{max} in comparison with Bi_2Te_3. The predicted PF_{max} is 2.80×10^{-3} W/mK^2, which approximately coincides with that for $x = 0.10$. The enhanced PF value is much larger than the optimum value with respect to the given carrier concentration. Therefore, we concluded that this enhancement may result from the proposed filtering effect. Here, the κ value for the $x = 0.10$ sample is not reduced in the nanocomposite, but the ZT value is higher than that for Bi_2Te_3 due to the high PF. Concerning the size of the filter phase, we found that micron-sized Ga_2Te_3 precipitates in Bi_2Te_3 do not affect PF_{max}. The PF_{max} for the $x = 0.2$ sample was much lower than that for the samples with $0.07 \le x \le 0.15$ because the TE properties of Ga_2Te_3 could not be ignored by increasing the volume ratio of Ga_2Te_3 to Bi_2Te_3. The appropriate amount of nanocomposites with the proper ΔE and W_0

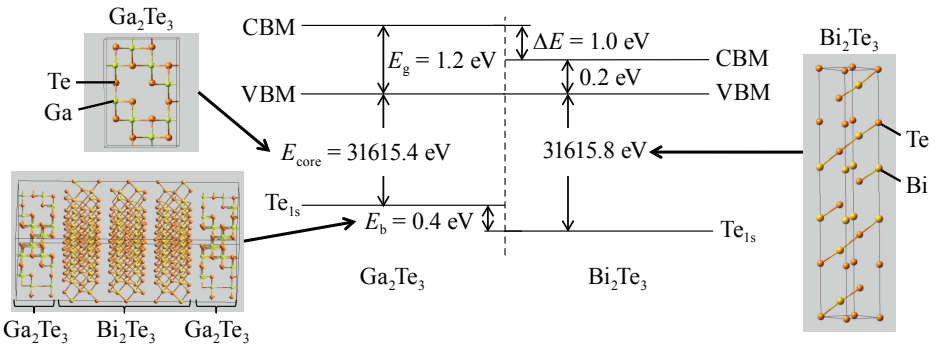

Fig. 9 Band offset between Ga_2Te_3 and Bi_2Te_3.[16] The crystal structure models for the Ga_2Te_3, Bi_2Te_3, and Bi_2Te_3/Ga_2Te_3 interface models (24 ($Ga_2Bi_4Te_9$)) used for the estimation of E_{core} or E_b are also shown.

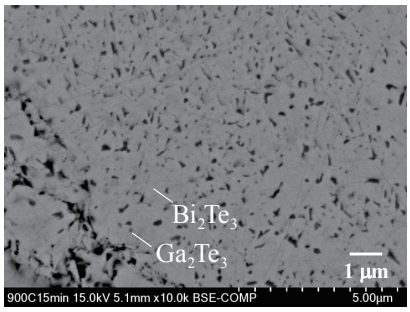

Fig. 10 Backscattered electron (BSE) image of the synthesized $Bi_{0.85}Ga_{0.15}Te_3$.[16]

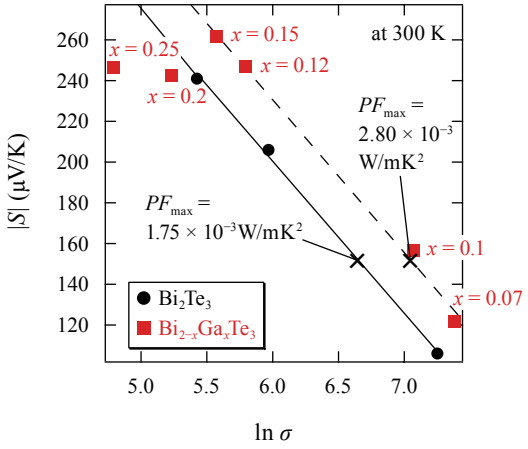

Fig. 11 Absolute value of the Seebeck coefficient ($|S|$) versus the natural logarithm of the electrical conductivity ($\ln \sigma$) for $Bi_{1-x}Ga_xTe_3$ ($0 \leq x \leq 0.25$) at 300 K.[16]

of the filter phase is effective for increasing *PF* beyond that obtained by optimizing the carrier concentration.

4. Conclusion

We investigated three conceptual ideas to improve the properties of TE materials. New TE materials were designed using first-principles calculations based on these three ideas and were then synthesized. Simultaneous co-doping with donors and acceptors in TiNiSn-based TE materials was first proposed. YSb co-doping increased the power factor due to the change in the band structure around the Fermi energy, as calculated. Crystallographic defects in TiNiSn-based TE materials were then studied. Interstitial Ni defects were produced by introducing excess Ni, which significantly lowered the thermal conductivity and improved the *PF*. Finally, an energy filtering effect for Bi_2Te_3-based TE materials was implemented using a Ga_2Te_3 filter phase selected by the calculations. Bi_2Te_3 with homogeneously dispersed nanosized Ga_2Te_3 precipitates was synthesized, and its maximum power factor was higher than that for Bi_2Te_3 due to the filtering effect. In all three cases, we obtained a significant improvement in the TE properties, thereby validating the strategy and emphasizing the importance of design concepts resulting from physical and chemical insights.

As mentioned in Sec. 1, TEGs are a green technology that are expected to be used in a variety of applications. However, the present TEG technology is still not mature for practical applications. Recently, we developed a solar TEG with a water heating system for efficiently using solar energy.[3] Here, we can consider the applicability of TE materials we have developed, such as $CoSb_3$-based[26] and sulfide[27,28] TE materials, as well as TiNiSn- and Bi_2Te_3-based TE materials. It is, however, necessary to ensure the performance, stability, and reliability of TEGs, especially under practical heat cycles. Thus, we need to study related technologies along with TE materials for commercial applications. In this context, extended studies are being performed, such as a search for electrodes with a low contact resistance and low thermal stress, and oxidation-resistant coating materials for TE materials.

Acknowledgements

The authors would like to thank Dr. Yamamoto, Dr. Suto, Dr. Kinoshita, and Dr. Ishikiriyama of Toyota Motor Corporation for their support in conducting the research in Sec. 3. 3.

References

(1) Crane, D., Lagrandeur, J., Jovovic, V., Ranalli, M., Adldinger, M., Poliquin, E., Dean, J., Kossakovski, D., Mazar, B. and Maranville, C., "TEG on-vehicle Performance and Model Validation and What It Means for Further TEG Development", *J. Electron. Mater.*, Vol. 42, No. 7 (2013), pp. 1582-1591.

(2) Kuroki, T., Kabeya, K., Makino, K., Kajihara, T., Kaibe, H., Hachiuma, H., Matsuno, H. and Fujibayashi, A., "Thermoelectric Generation Using Waste Heat in Steel Works", *J. Electron. Mater.*, Vol. 43, No. 6 (2014), pp. 2405-2410.

(3) Hazama, H., Masuoka, Y., Suzumura, A., Matsubara, M., Tajima, S. and Asahi, R., "Cylindrical Thermoelectric Generator with Water Heating System for High Solar Energy Conversion Efficiency", *Appl. Energy*, Vol. 226 (2018), pp. 381-388.
(4) Crane, D. T. and Lagrandeur, J. W., "Progress Report on BSST-led US Department of Energy Automotive Waste Heat Recovery Program", *J. Electron. Mater.*, Vol. 39, No. 9 (2010), pp. 2142-2148.
(5) Crane, D. T., Koripella, C. R. and Jovovic, V., "Validating Steady-state and Transient Modeling Tools for High-power-density Thermoelectric Generators", *J. Electron. Mater.*, Vol. 41, No. 6 (2012), pp. 1524-1534.
(6) Liu, W. S., Zhang, Q., Lan, Y., Chen, S., Yan, X., Zhang, Q., Wang, H., Wang, D., Chen, G. and Ren, Z., "Thermoelectric Property Studies on Cu-doped n-type $Cu_xBi_2Te_{2.7}Se_{0.3}$ Nanocomposites", *Adv. Energy Mater.*, Vol. 1, No. 4 (2011), pp. 577-587.
(7) Kim, S. I., Lee, K. H., Mun, H. A., Kim, H. S., Hwang, S. W., Roh, J. W., Yang, D. J., Shin, W. H., Li, X. S., Lee, Y. H., Snyder, G. J. and Kim, S. W., "Dense Dislocation Arrays Embedded in Grain Boundaries for High-performance Bulk Thermoelectrics", *Science*, Vol. 348, No. 6230 (2015), pp. 109-114.
(8) Shi, X., Yang, J., Salvador, J. R., Chi, M., Cho, J. Y., Wang, H., Bai, S., Yang, J., Zhang, W. and Chen, L., "Multiple-filled Skutterudites: High Thermoelectric Figure of Merit Through Separately Optimizing Electrical and Thermal Transports", *J. Am. Chem. Soc.*, Vol. 133, No. 20 (2011), pp. 7837-7846.
(9) Zong, P.-an, Hanus, R., Dylla, M., Tang, Y., Liao, J., Zhang, Q., Snyder, G. J. and Chen L., "Skutterudite with Graphene-modified Grain-boundary Complexion Enhances *zT* Enabling High-efficiency Thermoelectric Device", *Energy Environ. Sci.*, Vol. 10, No. 1 (2017), pp. 183-191.
(10) Zhang, Q., Liao, J., Tang, Y., Gu, M., Ming, C., Qiu, P., Bai, S., Shi, X., Uher, C. and Chen, L., "Realizing a Thermoelectric Conversion Efficiency of 12% in Bismuth Telluride/Skutterudite Segmented Modules through Full-parameter Optimization and Energy-loss Minimized Integration", *Energy Environ. Sci.*, Vol. 10, No. 4 (2017), pp. 956-963.
(11) Wu, D., Zhao, L.-D., Tong, X., Li, W., Wu, L., Tan, Q., Pei, Y., Huang, L., Li, J.-F., Zhu, Y., Kanatzidis, M. G. and He, J., "Superior Thermoelectric Performance in PbTe–PbS Pseudo-binary: Extremely Low Thermal Conductivity and Modulated Carrier Concentration", *Energy Environ. Sci.*, Vol. 8, No. 7 (2015), pp. 2056-2068.
(12) He, Y., Lu, P., Shi, X., Xu, F., Zhang, T., Synider, G. J., Uher, C. and Chen, L., "Ultrahigh Thermoelectric Performance in Mosaic Crystals", *Adv. Mater.*, Vol. 27, No. 24 (2015), pp. 3639-3644.
(13) Zhao, L.-D., Tan, G., Hao, S., He, J., Pei, Y., Chi, H., Wang, H., Gong, S., Xu, H., Dravid, V. P., Uher, C., Snyder, G. J., Wolverton, C. and Kanatzidis, M. G., "Ultrahigh Power Factor and Thermoelectric Performance in Hole-doped Single-crystal SnSe", *Science*, Vol. 351, No. 6269 (2016), pp. 141-144.
(14) Asahi, R., Morikawa, T., Hazama, H. and Matsubara, M., "Materials Design and Development of Functional Materials for Industry", *J. Phys.: Condens. Matter*, Vol. 20, No. 6 (2008), 064227.
(15) Hazama, H., Matsubara, M., Asahi, R. and Takeuchi, T., "Improvement of Thermoelectric Properties for Half-Heusler TiNiSn by Intersititial Ni Defects", *J. Appl. Phys.*, Vol. 110, No. 6 (2011), 063710.
(16) Hazama, H., Masuoka, Y., Yamamoto, H., Suto, H., Kinoshita, Y., Ishikiriyama, M. and Asahi, R., "Improvement of Power Factor of n-type Bi_2Te_3 by Dispersed Nanosized Ga_2Te_3 Precipitates", *J. Alloys Compd.*, Vol. 726 (2017), pp. 578-586.
(17) Hazama, H., Mizutani, U. and Asahi R., "First-principles Calculations of Ag-Sb Nanodot Formation in Thermoelectric $AgPb_mSbTe_{2+m}$ (m = 6, 14, 30)", *Phys. Rev. B*, Vol. 73, No. 11 (2006), 115108.
(18) Blöchl, P. E., "Projector Augmented-wave Method", *Phys. Rev. B*, Vol. 50, No. 24 (1994), pp. 17953-17979.
(19) Kresse, G. and Joubert, D., "From Ultrasoft Pseudopotentials to the Projector Augmented-wave Method", *Phys. Rev. B*, Vol. 59, No. 3 (1999), pp. 1758-1775.
(20) Kresse, G. and Furthmüller, J., "Efficient of Ab-initio Total Energy Calculations for Metals and Semiconductors Using a Plane-wave Basis Set", *Comput. Mater. Sci.*, Vol. 6, No. 1 (1996), pp. 15-50.
(21) Kresse, G. and Furthmüller, J., "Efficient Iterative Schemes for *Ab Initio* Total-energy Calculations Using a Plane-wave Basis Set", *Phys. Rev. B*, Vol. 54, No. 16 (1996), pp. 11169-11186.
(22) Sales, B. C., Mandrus, D., Chakoumakos, B. C., Keppens, V. and Thompson, J. R., "Filled Skutterudite Antimonides: Electron Crystals and Phonon Glasses", *Phys. Rev. B*, Vol. 56, No. 23 (1997), pp. 15081-15089.
(23) Tang, Y., Li, X., Martin, L. H. J., Reyes, E. C., Ivas, T., Leinenbach, C., Anand, S., Peter, M., Snyder, G. J. and Battaglia, C., "Impact of Ni Content on the Thermoelectric Properties of Half-Heusler TiNiSn", *Energy Environ. Sci.*, Vol. 11, No. 2 (2018), pp. 311-320.
(24) Tan, G., Zhao, L.-D. and Kanatzidis, M. G., "Rationally Designing High-performance Bulk Thermoelectric Materials", *Chem. Rev.*, Vol. 116, No. 19 (2016), pp. 12123-12149.

(25) Scheidemantel, T. J., Ambrosch-Draxl, C., Thonhauser, T., Badding, J. V. and Sofo, J. O., "Transport Coefficients from First-principles Calculations", *Phys. Rev. B*, Vol. 68, No. 12 (2003), 125210.
(26) Matsubara, M. and Asahi, R., "Optimization of Filler Elements in $CoSb_3$-based Skutterudites for High-performance *n*-type Thermoelectric Materials", *J. Electron. Mater.*, Vol. 45, No. 3 (2016), pp. 1669-1678.
(27) Suzumura, A., Nagasako, N., Kinoshita, Y., Watanabe, M., Kita, T. and Asahi, R., "Presence of a Doubly-splitting Site and Its Effect on Thermoelectric Properties of Cu_4SnS_4", *Mater. Trans.*, Vol. 56, No. 6 (2015), pp. 858-863.
(28) Suzumura, A., Watanabe, M., Nagasako, N. and Asahi, R., "Improvement in Thermoelectric Properties of Se-free Cu_3SbS_4 Compound", *J. Electron. Mater.*, Vol. 43, No. 6 (2014), pp. 2356-2361.

Hirofumi Hazama
Research Fields:
- Material Science
- Solid-state Physics

Academic Degree: Dr.Sci.
Academic Societies:
- The Physical Society of Japan
- The Japan Society of Applied Physics

Masato Matsubara
Research Fields:
- Inorganic Synthesis Chemistry
- Combinatorial Chemistry

Academic Degree: Dr.Eng.

Yumi Masuoka
Research Field:
- Material Science

Academic Society:
- The Japan Society of Applied Physics

Ryoji Asahi
Research Fields:
- Materials Informatics
- Computational Materials Design

Academic Degree: Ph.D.
Academic Societies:
- The Japan Society of Applied Physics
- The Japan Institute of Metals and Materials
- American Physical Society

Award:
- Technical Development Award, The Chemical Society of Japan, 2006